Int J Adv Manuf Technol (2017) 89:3563–3578
DOI 10.1007/s00170-016-9357-y

ORIGINAL ARTICLE

FE prediction of thermal performance and stresses in an automotive disc brake system

Ali Belhocine[1]

Received: 30 May 2016 / Accepted: 15 August 2016 / Published online: 23 August 2016

Abstract This study aims to identify thermal effects in the structure and the contact behavior of a disc-pad assembly using a finite element approach. The first analysis is performed on the disc-pad model in the absence of thermal effects. The structural performance of the disc-pad model is predicted in terms of factors such as the deformation and von Mises stress. Next, thermomechanical analysis is performed on the same disc-pad model with the inclusion of convection, adiabatic, and heat flux elements. The predicted temperature distribution, deformation, stress, and contact pressure are presented. The structural performance between the two analyses (mechanical and thermomechanical) is compared. For this contribution, we were able to find and use some experimental results on the contact pressure distributions inner brake pads to validate our thermomechanical model. This study can assist brake engineers in choosing a suitable analysis method to critically evaluate the structural and contact behavior of the disc brake assembly.

Keywords Finite element · Disc-pad model · Temperature · Deformation · Stress · Contact pressure

1 Introduction

During basic operation, a disc or drum brake system has to reduce the wheel speed when a driver desires vehicle deceleration. The kinetic energy generated by a vehicle in terms of wheel speed is converted into heat energy owing to the application of the brake system. Braking system acts as one of the most fundamental safety-critical components in modern passenger cars. Therefore, the braking system of a vehicle is a significant system, especially in slowing down or stopping the vehicle [1]. The friction force between the disc/drum and the brake pad/brake shoe applies friction torque to the wheel in the opposite direction of the car's movement. This results in the reduction of the vehicle speed, and the production of heat energy in the brake disc/drum causes a temperature increase in the disc/drum swept area during brake application. This physical action of the brake disc/drum causes heat conduction to the adjacent braking system components, as referred to in [2].

Kumar and Vinodh [3] used the finite element method for both static structural and transient thermal analysis while proposing a new automotive brake rotor design and compared it with a ventilated disc brake rotor. This analysis was conducted to visualize the stress and deformation pattern of the rotors under extreme loads. Agnihotri and Chopra [4] presented a newly developed model to predict the temperature rise and temperature behavior of a solid and a ventilated disc brake rotor. Their study aimed to investigate the heat and temperature distribution in the disc brake rotor. Analysis System (ANSYS) has been used as finite element software to perform thermostructural analysis on the disc brake. The disc materials used in this simulation are stainless steel and gray cast iron. Both results have been estimated with better justification. Parab et al. [5] presented a thermomechanical analysis of a disc brake using three materials: stainless steel, cast iron, and carbon composite. The modeling was based on CATIA. Two analyses were conducted for validating the strength of the disc brake and the thermal properties. The best material among the three was identified by comparing the deformation, stresses, temperature, etc. Gao and Lin [6] and Gao et al. [7] investigated the transient temperature field and thermal fatigue fracture of the solid disc of a 3D thermomechanical coupling analysis. Hwang et al. [8]

✉ Ali Belhocine
al.belhocine@yahoo.fr

[1] Faculty of Mechanical Engineering, University of Sciences and the Technology of Oran, L.P 1505 El - MNAOUER, USTO, 31000 Oran, Algeria

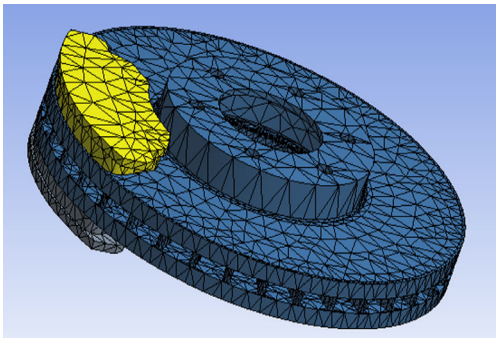

Fig. 1 FE model of a disc-pad assembly

performed thermomechanical coupled analysis and developed a multibody model for repeated braking to predict the temperature field of a ventilated brake disc. Their study aimed to discuss the nonuniform temperature distribution. Choi and Lee [9] studied the thermoelastic behavior of a disc brake during repeated braking using a 2D thermomechanical coupling model. Belhocine and Bouchetara [10] used the finite element software ANSYS 11.0 to study the thermal behavior of full and ventilated disc brake rotor. Recently, Belhocine and Wan Omar [11] conducted a study using finite element (FE) to investigate the structural and mechanical behavior of a three-dimensional disc-pad model during the braking process under dry contacts slipping conditions.

The novelty of this work is to demonstrate the effect of temperature on the thermomechanical response of the disc due to the interaction between deformation and temperature field. For this reason, it may be interesting to combine the thermal effects to mechanical effects. It was during the stop phases of deceleration that the brake discs are subjected to mechanical and thermal stresses due to friction pads and brake discs. Indeed, in the vehicle braking process, the temperature fields induce significant thermal stresses, and these constraints must be taken into account by adding to the mechanical stresses.

For this purpose, depth comparative study of the results of the analysis with and without thermal effect was conducted by the author who has never been previously treated.

The present study aimed to investigate the structural and contact behaviors of the brake disc and pads during the braking phase with and without thermal effects. Finite element analysis was employed for both static structural and transient thermal analysis. First, the total deformation of the disc-pad model at the time of braking and the stress and contact distributions of the brake pads were determined. Then, the results of thermoelastic coupling, such as von Mises stress, contact pressure field, and total deformations of the disc and pads, were presented.

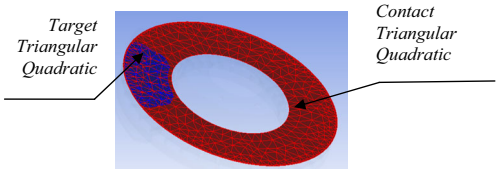

Fig. 2 Contact zone of the disc and pad

Table 1 Finite element mesh properties

Description	Nodes	Elements
Disc	34799	18268
Pad 1	1446	650
Pad 2	1461	660
Contact zone 1	0	914
Contact zone 2	0	83

Finally, experimental results found in the literature under the same conditions of braking were used to confirm contacting pressure distribution predicted in the FE model. These will be useful in the brake design process for the automobile industry.

2 Finite element (FE) model and assumptions

The unsteady heat conduction equation of each body for an axis-symmetric problem described in the cylindrical coordinate system is given as follows:

$$\rho c \frac{\partial T}{\partial t} = \frac{1}{r}\frac{\partial}{\partial r}\left(r k_r \frac{\partial T}{\partial r}\right) + \frac{\partial}{\partial z}\left(k_z \frac{\partial T}{\partial z}\right) \quad (1)$$

With the boundary conditions and initial condition

$$T = T^* \text{ on } \Gamma_0 \quad (2)$$

$$q_n = h(T - T_\infty) \quad \text{on } \Gamma_1 \quad (3)$$

$$q_n = q_n^* \quad \text{on } \Gamma_2 \quad (4)$$

$$T = T_0 \quad \text{at time} = 0 \quad (5)$$

where ρ, c , and k_r and k_z are the density, specific heat, and thermal conductivities in r and z direction of the material, respectively. Also, T^* is the prescribed temperature, h the heat transfer coefficient, q_n^* the heat flux at each contact interface due to friction, T_∞ the ambient temperature, T_0 the initial temperature, and Γ_0, Γ_1, and Γ_2 are the boundaries on which temperature, convection, and heat flux are imposed, respectively.

Table 2 Thermoelastic properties of the disc and pad

	Disc	Pad
Young modulus E (GPa)	138	1
Poisson's ratio υ	0.28	0.25
Density ρ(kg/m^3)	7250	1400
Coefficient of friction μ	0.2	0.2
Thermal conductivity, k (W/m °C)	57	5
Specific heat, c (J/kg °C)	460	1000
Angular velocity, ω (rad/s)	157.89	
Hydraulic pressure, P (MPa)	1	

Table 3 Design parameters of the disc and pads

	Disc	Pad
Volume (m^3)	9.5689e−004	8.5534e−005
Surface (m^2)	0.24237	1.8128e−002
Mass (kg)	6.9375	0.44975
Inertia moment Ip1 (kg m^2)	3.5776e−002	2.7242e−005
Inertia moment Ip2 (kg m^2)	6.9597e−002	1.5131e−004
Inertia moment Ip3 (kg m^2)	3.5774e−002	1.2863e−004

Using Galerkin's approach, a finite element formulation of unsteady heat Eq. (2) can be written in the following matrix form as

$$C_T\dot{T} + \mathrm{KH}_T T = R \tag{6}$$

where C_T is the capacity matrix, KH_T is the conductivity matrix. T and R and are the nodal temperature and heat source vector, respectively.

The most commonly used method for solving Eq. (6) is the direct integration method based on the assumption that temperature T_t at time t and temperature $T_{t+\Delta t}$ at time $t+\Delta t$ have the following relation:

$$T_{t+\Delta t} = T_t + \left[(1-\beta)\dot{T}_t + \beta\dot{T}_{t+\Delta t}\right]\Delta t \tag{7}$$

Eq. (7) can be used to reduce the ordinary differential Eq. (6) to the following implicit algebraic equation:

$$(C_T + b_1 KH_T)T_{t+\Delta t} = (C_T - b_2 KH_T)T_t + b_2 R_t + b_1 R_{t+\Delta t} \tag{8}$$

where the variables b_1 and b_2 are given by

$$b_1 = \beta\Delta t, b_2 = (1-\beta)\Delta t \tag{9}$$

For different values of β, the well-known numerical integration scheme can be obtained [12] in this study, $0.5 \le \beta \le 1.0$ was used, which is an unconditionally stable scheme.

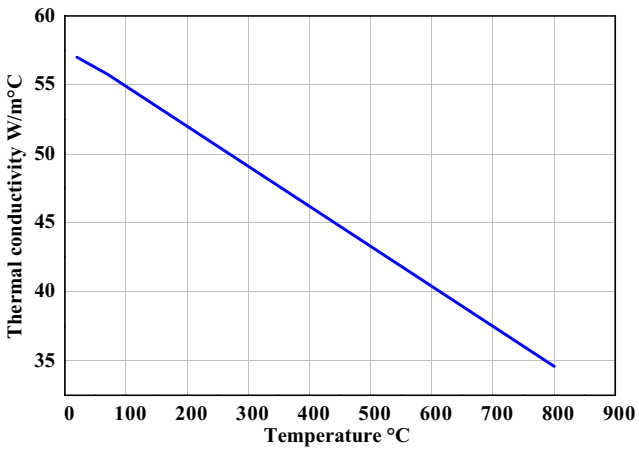

Fig. 3 Thermal conductivity versus temperature

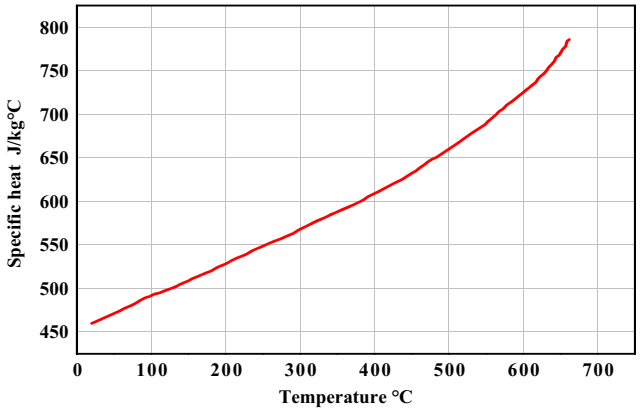

Fig. 4 Specific heat versus temperature

The main problem of braking and stopping an automotive system is the great input of heat flux into the disc in a very short time. Because of the high temperature difference, the material is exposed to high stress. The result is a heat shock. Because the disc brake and pads are the main components involved thermically and mechanically during braking, the present study excludes other vital components such as the pistons and caliper from the analysis.

In this study, a three-dimensional FE model consisting of a ventilated disc and two pads is employed, as illustrated in Fig. 1. Figure 2 shows the contact zones between the disc and the pad. Table 1 lists details about the mesh properties.

The disc is made of gray cast iron FG 15 with high carbon content. The brake pad shows isotropic elastic behavior. Tables 2 and 3, respectively, list the mechanical characteristics and design parameters of these two parts. ANSYS 11 (3D), commercial FE software, is used to simulate the structural deformation, stress, temperature, and contact pressure distributions of the disc brake during braking.

Rotors are made of cast iron for following three reasons [13]:

- It is relatively hard and resists wear.
- It is cheaper than steel or aluminum.
- It absorbs and dissipates heat well to cool the brakes.

It is very difficult to exactly model the brake disc, in which there are still researches going on to find out the transient thermal behavior of disc brake during braking applications. There is always a need of some assumptions to model any

Table 4 Vehicle data

Vehicle mass—M (kg)	1385
The initial velocity v_0 (m/s)	60
Duration of braking application (s)—t_{stop}	45
The effective radius of the disc—(mm)	100.5
The radius of the wheel—(mm)	380
Friction coefficient disc/pad μ (/)	0.2
Pad surface A_d (mm^2)	5246.3
Rotor force F_{disc} (N)	1047.36

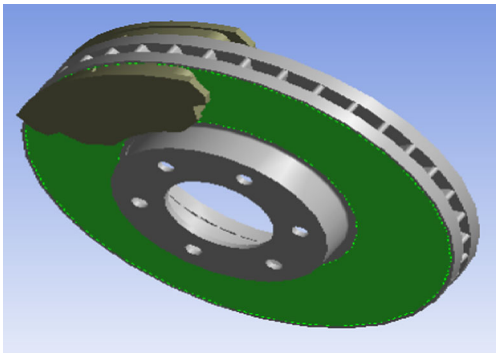

Fig. 5 Contact surface of the disc

complex geometry. These assumptions are made, keeping in mind the difficulties involved in the theoretical calculation and the importance of the parameters that are taken and those which are ignored. In modeling, we always ignore the things that are of less importance and have little impact on the analysis. The assumptions are always made depending upon the details and accuracy required in modeling.

Due to the application of brakes on the car disc brake rotor, heat generation takes place due to friction and this thermal flux has to be conducted and dispersed across the disc rotor cross section. The condition of braking is very much severe and thus the thermal analysis has to be carried out. The thermal loading as well as structure is axis-symmetric. Hence, axis-symmetric analysis can be performed, but in this study, we performed 3D analysis, which is an exact representation for this thermal analysis. Thermal analysis is carried out and with the above load structural analysis, is also performed for analyzing the stability of the structure.

To simplify the analysis, several assumptions have also been made as follows [14]:

- All kinetic energy at disc brake rotor surface is converted into frictional heat or heat flux.
- The heat transfer involved for this analysis is only conduction and convection process. This heat transfer radiation can be neglected in this analysis because of small amount which is 5 to 10 % [15].
- The disc material is considered as homogeneous and isotropic.

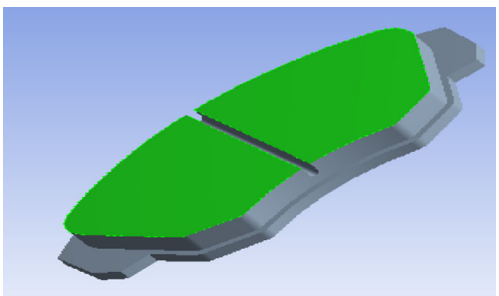

Fig. 6 Contact surface of the pad

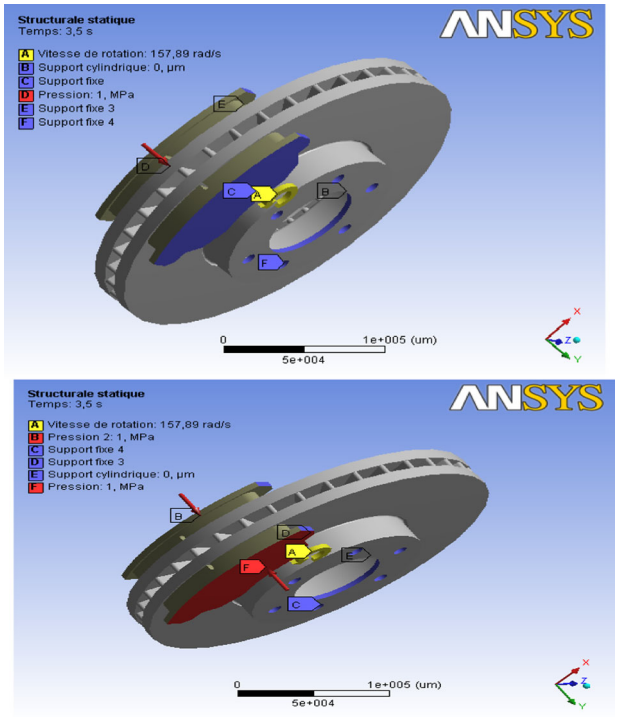

(a) One side (b) Two sides

Fig. 7. Boundary conditions and loading imposed on the disc-pads. **a** One side. **b** Two sides

- The domain is considered as axis-symmetric.
- Inertia and body force effects are negligible during the analysis.
- The disc is stress free before the application of brake.
- In this analysis, the ambient temperature and initial temperature have been set to 20 °C
- All other possible disc brake loads are neglected.
- Only certain parts of the disc brake rotor will apply with convection heat transfer such as cooling vane area, outer ring diameter area, and disc brake surface.
- Uniform pressure distribution by the brake pad onto the disc brake surface.

The thermal conductivity and specific heat are a function of temperature (Figs. 3 and 4).

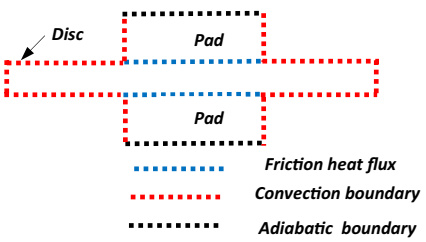

Fig. 8 Boundary condition for thermal analysis of the disc brake

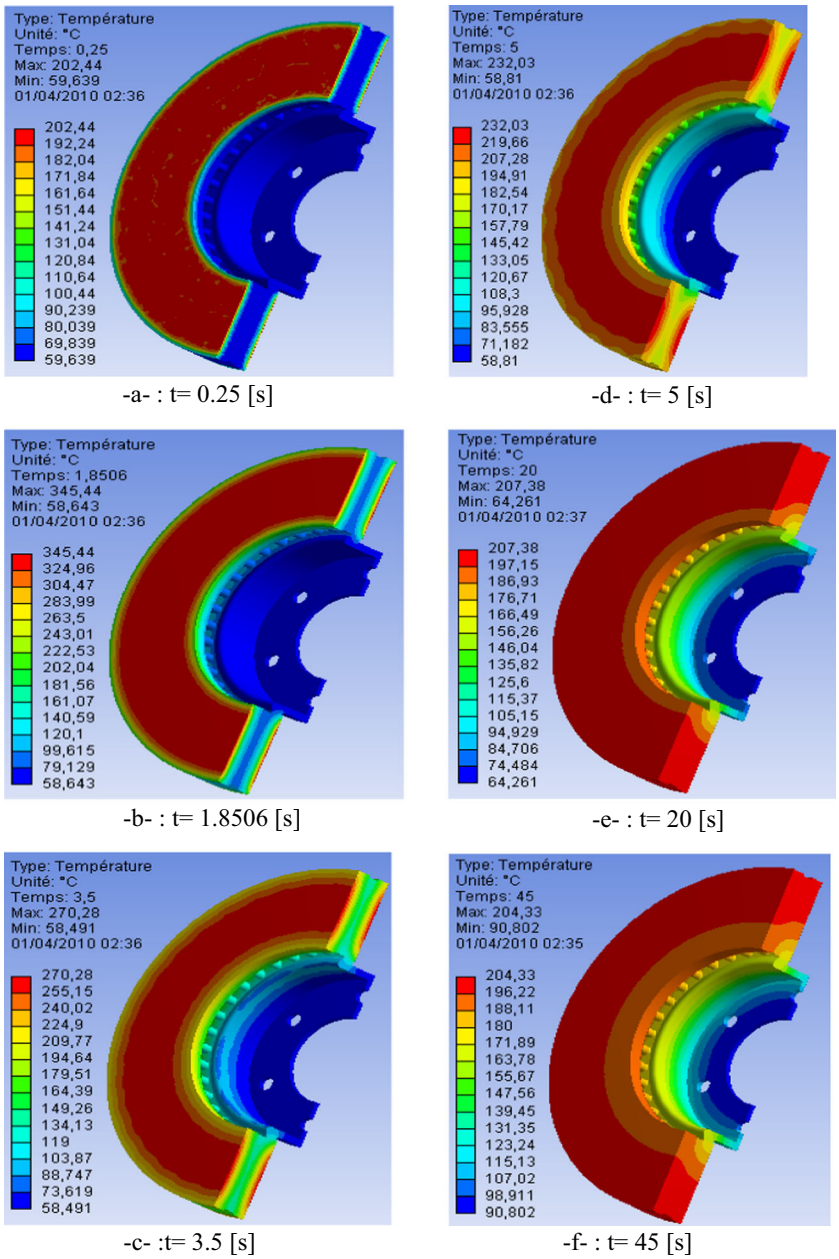

Fig. 9 **a**–**f** Temperature distribution for a ventilated disk of material FG 15

2.1 Force determination for the brake caliper

In this study, the initial mechanical calculation aims at determining the value of the contact pressure (presumably constant) between the disc and the pad. It is assumed that 60 % of the braking forces are supported by the front brakes (both discs), i.e., 30 % for a single disc, as cited in [16]. The force of the disc for a typical vehicle is calculated using the vehicle data listed in Table 4 to obtain the working forces on the brake disc:

$$F_{\text{disc}} = \frac{(30\%) \times \frac{1}{2} M v_0^2}{2 \times \frac{R_{\text{rotor}}}{R_{\text{tire}}} \left(v_0 \times t_{\text{stop}} - \frac{1}{2} \left\{ \frac{v_0}{t_{\text{stop}}} \right\} t_{\text{stop}}^2 \right)} \tag{10}$$

The rotational speed of the disc is calculated as follows:

$$\omega = \frac{v_0}{R_{\text{tire}}} \tag{11}$$

The total disc surface in contact with the pads is 35,797 mm^2, as shown in Fig. 5.

The surface pressure between the disc and the pad for the calculated force applied to the disc needs to be determined. For braking on a flat track, the pressure is given as follows [17]:

$$P = \frac{F_{\text{disc}}}{A_c \times \mu} \tag{12}$$

where A_c is the surface area of the pad in contact with the disc and μ is the friction coefficient. The surface area of the pad in contact with the disc in mm^2 is given directly in ANSYS by selecting this surface, as indicated by the green color in Fig. 6. For a brake pad without a groove, the hydraulic pressure is calculated in the same manner.

2.2 Mechanical boundary conditions

2.2.1 Disc boundary conditions

In our three-dimensional FE model, the disc is firmly attached to the clamp holes, on which it turns with a constant angular velocity ω = 157.89 rad/s. Fixed cylindrical support is applied to the internal diameter of the disc according to two axial and radial directions by leaving the free tangential direction.

2.2.2 Pads boundary conditions

The structural boundary conditions applied to the pads are defined as follows:

- The pad is embedded on its edges on the level of the orthogonal plane on the contact surface. All edges of the pad are constrained to only permit rigid body motion of the pad in a direction normal to the *XZ*-plane.
- A fixed support is imposed on the finger pad.
- The piston pad is subjected to a pressure of 1 MPa.
- A friction coefficient of 0.2 defines contact rubbing between the disc and the pads.

In this FE model, boundary conditions are imposed on the models (disc-pad) as shown in Figs. 7a, b, respectively, for applied pressure on one and both sides of the pad. The inner and outer pads, respectively, ride on the inside and outside of the brake rotor. The disc is rigidly constrained at the bolt holes

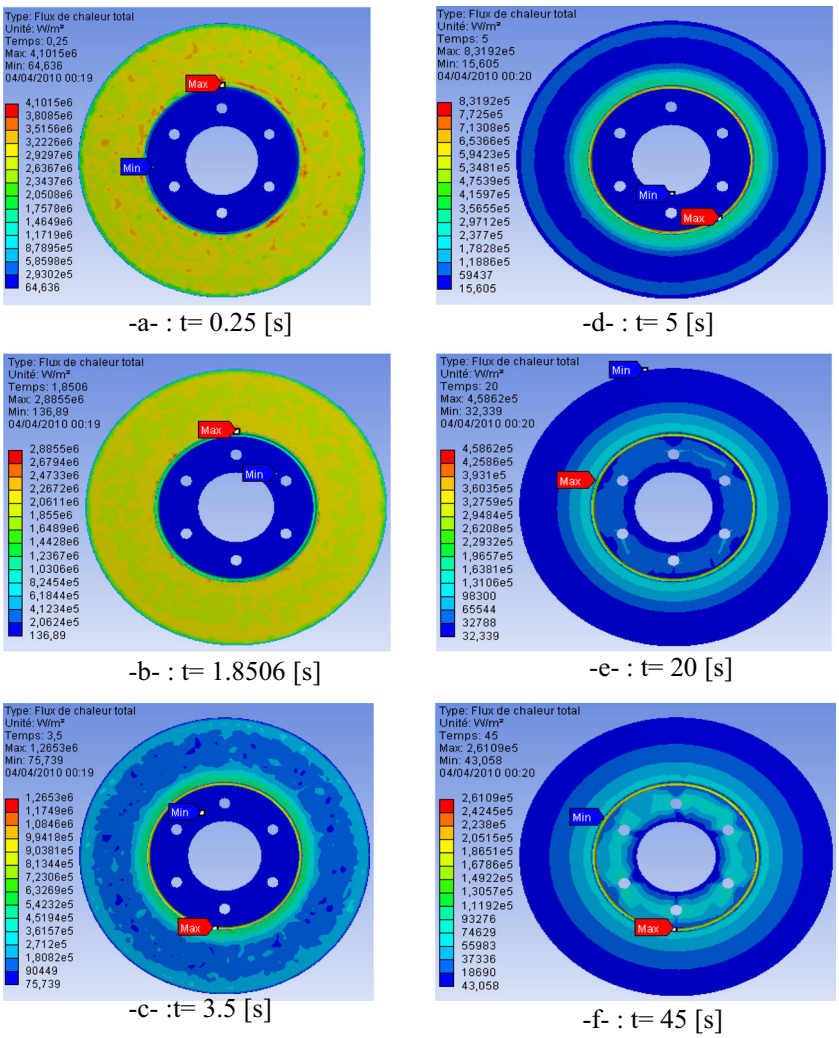

Fig. 10 **a**–**f** Distribution of total heat flux for a ventilated disk of material FG 15

in all directions except in its rotational direction. Meanwhile, the pad is fixed at the abutment in all degrees of freedom except in the normal direction to allow the pads to move up and down and in contact with the disc surface.

2.3 Thermal boundary conditions

For the prediction of the temperature variation of the brake disc excited by axial and radial deformation, a fully coupled thermomechanical model is used in this simulation. Conduction and convection are the two heat transfer modes considered in this study. The heat transfer coefficient by convection is imposed on all surfaces of the disc, and the radiation mode is considered negligible.

To express the heat transfer in the disc brake model, the thermal boundary conditions and initial condition have to be defined. At the interface between the disc and the brake pads, heat is generated owing to sliding friction, as indicated by the dashed in Fig. 6. In the exposed region of the disc and brake pads, it is assumed that heat is exchanged with the environment through convection, as cited in [18]. The backplate of the pad is an important parameter for the heat flux to the fluid. This backplate and shim is usually composed of different material layers to isolate the fluid as much as possible and to guide as much heat as possible to the caliper. Therefore, a large difference in the thermal resistance of the backplate can exist between two different pad types. Therefore, the convection surface boundary condition is applied there. On the surface of the back plate, an adiabatic or insulated surface boundary condition is used and shown in Fig. 8.

3 Finite element results and discussion

3.1 Temperature and heat flux distribution in ventilated disc

In this part, one presents the cartographies of total and directional heat flux and as well as the temperature distribution in a ventilated disk and of cast iron FG 15 for each moment with braking as indicated in Fig. 9. The temperature distribution of the disk at the beginning of braking (with $t = 0.25$ s) is inhomogeneous. According to experimental tests carried out by research, braking often begin with the formation from hot circles relatively on the uniform surfaces of the disc in the circumferential direction, moving radially on the disk and transforming them into hot points (*hot spot*). The appearance of the phenomenon of the hot points is due to the nonuniform dissipation of heat flux.

Concerning the heat flux, one notes according to Figs. 10 and 11 that the maximum value of the total heat flux is located on the level of the calorific throat at the end of braking ($t = 3.5$ s); this is explained by the increase in the gradients and the thermal concentrations in this zone. The calorific throat is manufactured so as to limit the heat flux coming from the friction tracks and moving towards the bowl of the disk brake in order to avoid the excessive heating of the rim and the tire. During the heating, the disk is tightened to dilate in the hot zones from where creating of compressive stresses with plasticization. On the other hand, during cooling, there is appearance of residual stresses of traction. The disk is thus subjected during its rotation to constraints traction/compression.

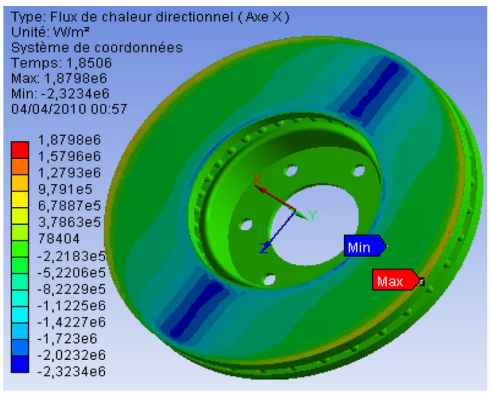

-a- : According to the axis X

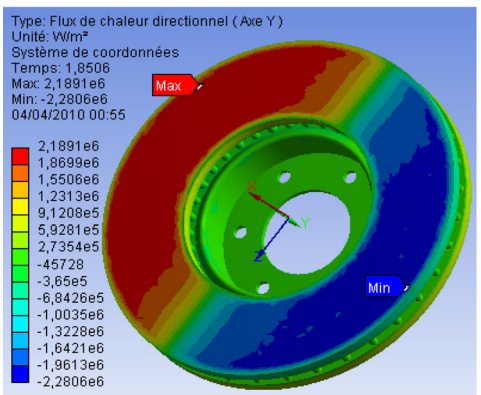

-b- : According to the axis Y

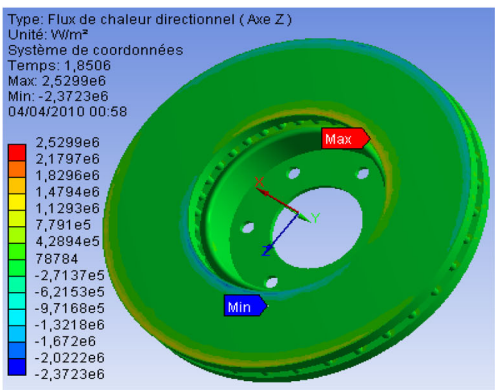

-c- : According to the axis Z

Fig. 11 **a**–**c** Distribution of directional heat flux at the moment $t = 1.8506$ (s) according to three axes (X, Y, Z) for a ventilated disk of a material FG 15

3.2 Predictive FE model in structural contact analysis

The computer code ANSYS also allows the determination and visualization of the structural deformations owing to the sliding contact between the disc and the pads. The results of the calculations of the contact described in this section relate to displacements or the total deformation during the loading sequence, the field of equivalent von Mises stress on the disc, and the contact pressures of the inner and outer pads at different braking periods.

3.2.1 Structural distortion of disc-pad model

Figure 12a–f show the disc deformations against the braking time. It is noted that large deformation is always found at the outer radius of the disc; this is the area in contact with the pad. These figures show that the highest deformation is 53 μm, and it is predicted at a braking time of t = 3.5 s and onwards. For pads, the highest deformation is located at the outer radial region (visualized in red), as shown in Fig. 13. Furthermore, the pads are less deformed compared to the disc, as shown in Figure 14. It is noted that the part most requested in loading gives displacements more significant than the other areas. The inner pad subjected to hydraulic pressure has a larger deformation than the disc. This behavior is also shown by the disc and outer pad. At a braking time of t = 3.5 s and onwards, the maximum deformation of the pads is predicted to be 19 μm, which is 64 % lower than that of the disc. This is due to the structural stiffness and type of constraints that have been assigned to the disc and pads.

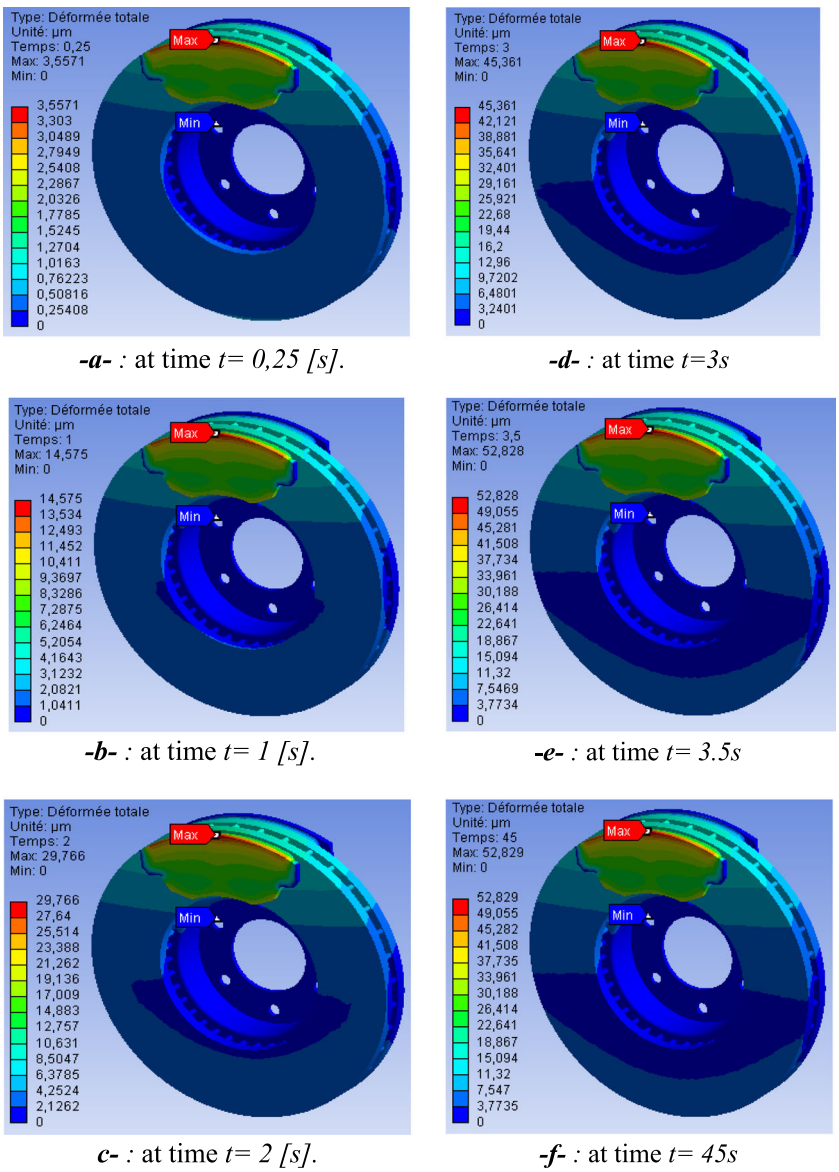

-a- *: at time t= 0,25 [s].*

-d- *: at time t=3s*

-b- *: at time t= 1 [s].*

-e- *: at time t= 3.5s*

c- *: at time t= 2 [s].*

-f- *: at time t= 45s*

Fig. 12 **a**–**f** Disc deformation at different braking time

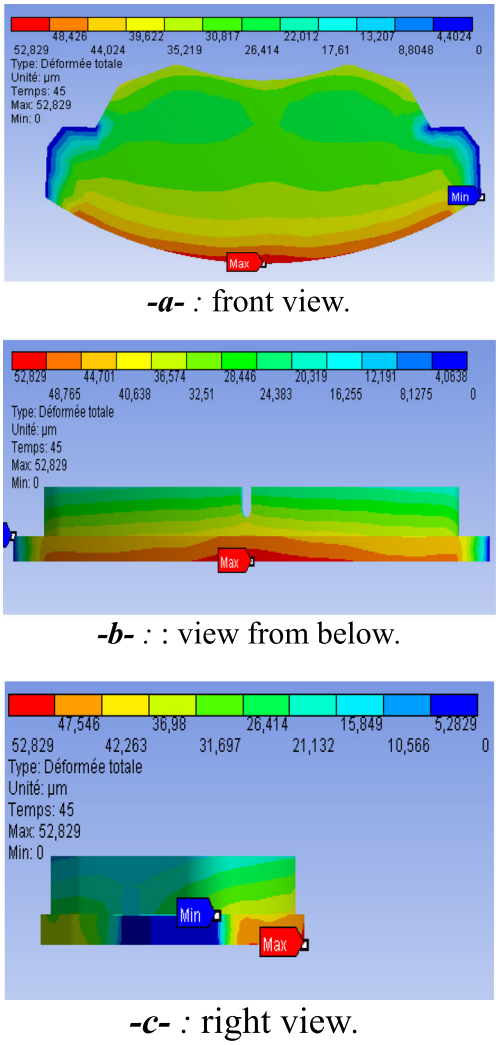

Fig. 13 **a**–**c** Pad deformation at braking time $t = 45$ s

3.2.2 *von Mises stress at pad*

Figure 15a–h shows that the equivalent von Mises stress is distributed almost symmetrically between the leading and the trailing side of the pad. These stress distributions are barely unchanged over braking time, except for the stress value. The stress increases gradually and reaches its maximum value of 5.3 MPa at a braking time of 3.5 s and onwards. The highest stress is predicted on the left side and the outer radius of the pad, whereas the lowest stress is located on the lower radius of the pad and near the groove area. Figure 16 shows a clear picture of the stress distributions at a braking time of $t = 45$ s across the inner pad contact surface. More uniform stress distribution occurs at the lower radius of the pad compared to the outer radius and center region of the pad. In addition, the highest stress is generated on the right and left sides at the outer radius and center region of the pad, respectively.

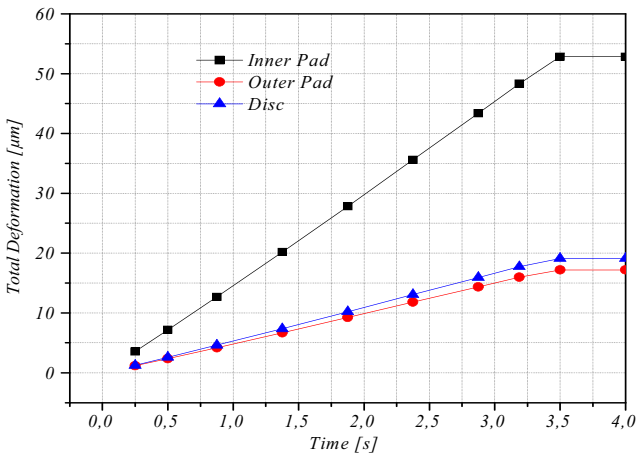

Fig. 14 Deformation of the disc and pads at different braking period

3.3 Predictive FE model in thermomechanical coupling analysis

In this section, structural and transient thermal analyses are coupled using ANSYS Multiphysics to identify the stress levels and global deformations of the model studied during the braking phase under the effect of temperature.

3.3.1 *Temperature distribution*

The initial temperature of the disc and pads is set at 20 °C, surface convection condition is applied to all surfaces of the disc, and convection coefficient of 5 W/m^2 °C is applied at the surface of the two pads. For the disc, the current authors have previously estimated [10] the values of the convective heat transfer coefficient in the shape of the curves for each surface of the rotor varying according to time. Figure 17 shows that at a braking time of 1.7 s, the disc and pad surface generate a very high temperature of 346 °C. However, the upper part of the backplate shows a lower temperature of ~90 °C. This is caused by the convection of ambient air.

3.3.2 *Thermoelastic distortion and von Mises stress of disc-pad model*

The aim of this coupled structural-thermal analysis is to gain a better understanding of the total deformation of the disc when it is not only subjected to load from the pads but also the expansion induced by the effect of temperature. Figure 18 shows the disc deformations at the nodes located in the mean and outer radius of the disc. A clear difference in disc deformation can be found between these two regions, where the outer radius of the disc shows higher deformation than the mean radius. The curves indicate an umbrella phenomenon that results from the heating of the nonparallel paths of friction with respect to the initial position. Figure 19 shows that the disc deformation increases linearly as a function of the disc

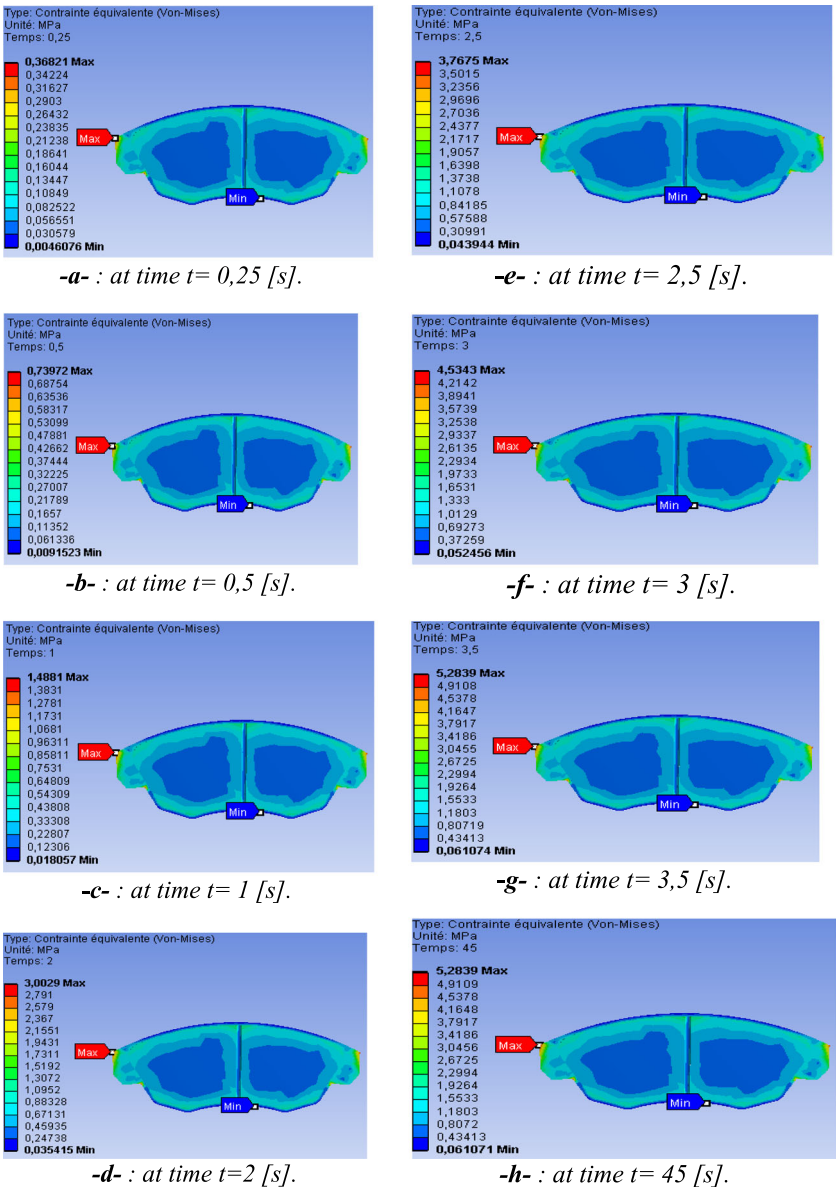

Fig. 15 **a**–**h** Von Mises stress distribution of the pad over braking time

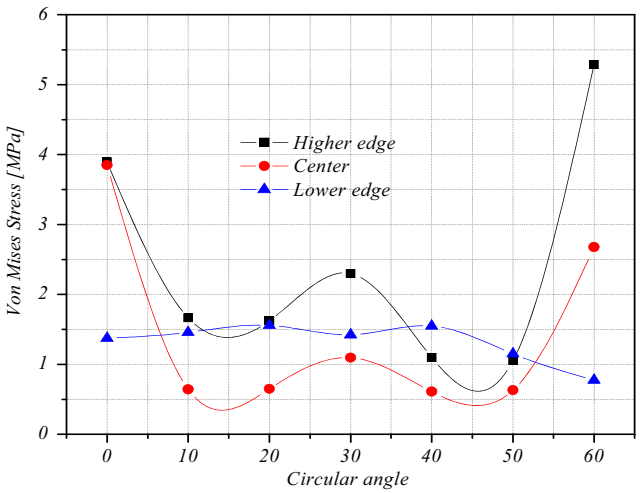

Fig. 16 von Mises stress at different angular positions of the pad

radius. The highest deformation is predicted at an angular position of 90° and the lowest deformation, at 270°.

The result shows that there is a significant difference between the mechanical and the thermoelastic model in terms of

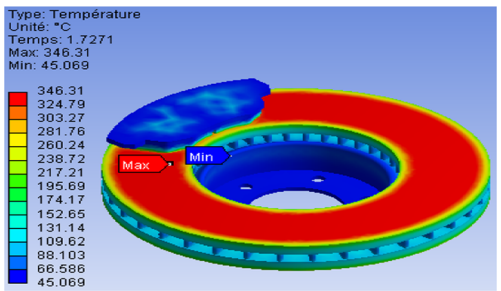

Fig. 17 Temperature distribution of the disc and pads at braking time $t = 1.7$ s

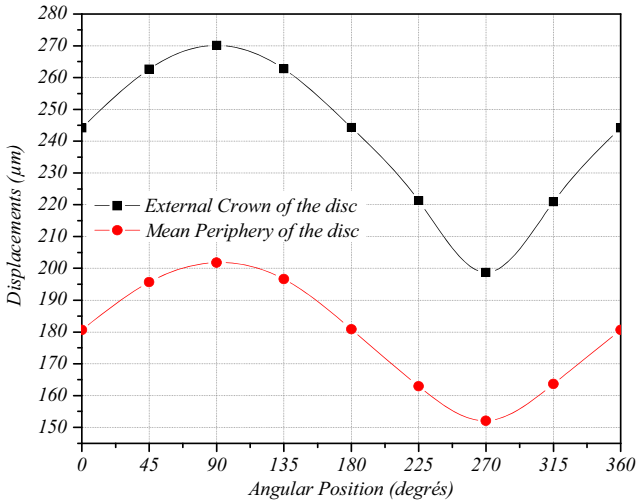

Fig. 18 Disc deformation at the mean and outer radius over angular positions at braking time $t = 3.5$ s

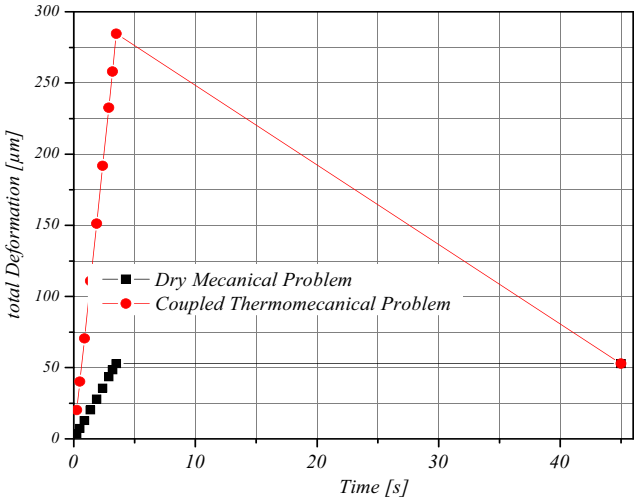

Fig. 20 Disc deformation with and without thermal effects

deformation and contact pressure. Figure 20 shows that the disc deforms severely under the effect of temperature. For instance, at a braking time of 3.5 s, the discs with and without the thermal effect deform by 280 and 53 µm, respectively. This clearly indicates that temperature strongly influences the thermomechanical response of the brake disc. During a braking maneuver, the maximum temperature achieved on the tracks depends on the storage capacity of the thermal energy in the disc. Indeed, the frictional heat generated on the rotor surface can induce excessive temperature rise that in turn leads to undesirable effects such as thermal elastic instability (TEI), premature wear, brake fluid vaporization, and thermally excited vibrations. The temperature distribution depends on various factors such as friction, surface roughness, and speed. The effect of the angular velocity and contact pressure induces the temperature rise of the disc brake. Figure 21 shows that the maximum displacement is localized on the slopes of friction, fins, and outer ring. Indeed, the brake discs are found to suffer from three main problems during servicing: cracking, wear, and distortion. Two types of distortion can occur during brake operation. The first is caused by the high mechanical forces acting on the disc during heavy braking and the transmission of braking torque to the axle. The second, and main, form of disc distortion is thermal deformation arising from large temperature differences across the disc owing to heavy braking. Four basic types of thermal deformation occur in discs: radial expansion, coning, waving, and rippling.

This phenomenon is due to the fact that the deformation of the disc is caused by heat (umbrella effect) that can lead to cracking of the disc. In this case, thermocoupling analysis is quite important to determine where thermal gradients and expansions generate thermal stresses in addition to the mechanical stress.

3.3.3 von Mises stresses at inner pad

Loading in a single piston is located at one side of the caliper only. Hydraulic pressure from the master cylinder is applied to the piston, as a result of which it presses the inner pad against

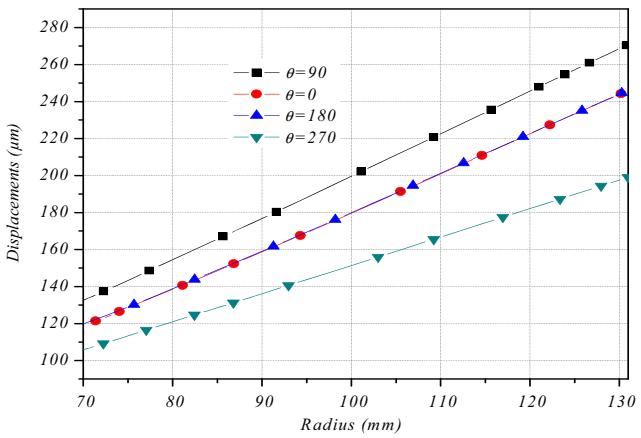

Fig. 19 Disc deformation at different radius and angular positions at braking time $t = 3.5$ s

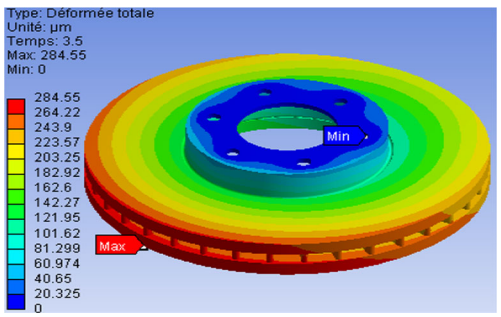

Fig. 21 Maximum total deformation of the disc with thermomechanical coupling

the disc rotor (see Fig. 7a). Loading with a double piston is located on both sides of the caliper and provides equal force to each pad (see Fig. 7b).

In this section, the influence of the pad groove and loading modes (single and dual piston) on the equivalent Von Mises stress distribution is presented. Figure 22a–g shows the stress evolution for three pad designs. At the beginning of braking (t = 1.7 s), most of the pad contact surfaces are dark blue, indicating lower stress. However, by a braking time of t = 4.5 s, the stress level increases and the color becomes almost ocean blue. At this braking time, the three pad designs clearly show different stress distributions. The presence of the groove and double piston loading has a positive effect on the stresses of the pad.

The results from the ANSYS simulation are listed in Table 5.

A comparison of the different results of the von Mises stress field shows that the pads without a groove for double piston loading show reducedstress. Accordingly, such pads are considered ideal for the present application.

3.3.4 Contact pressure distribution

Owing to thermal deformation, the contact area and therefore the pressure distribution also change. Thermal and mechanical deformations affect each other strongly and simultaneously. The pressure distribution at the disc-pad interface affects brake noise generation in three ways. First, it affects wear through friction; wear, in turn, alters the pressure distribution. Second, the contact stiffness and friction force depends on the level of contact pressure. Third, in the region of the pad surface where there is no contact pressure; there is no interaction between that region and the disc. In fact, fluctuating contact pressure (and therefore fluctuating friction force) can excite a brake system into resonance. The contact pressure distribution plotted in Fig. 23 is based on a braking time of t = 1.7 s, where the pad surface temperature is T = 346 °C. It is seen that the contact pressure curves are almost identical in shape for three different regions of the pad. At 30° angle, the contact pressure is predicted to be higher at lower pad radius followed by the outer pad radius and middle pad radius. The most significant outcome is to see the effect of temperature on the contact pressure of the disc-pad model. The thermal distortion of a normally flat surface into a highly deformed state is called thermoelastic transition. It occasionally occurs when the operating conditions of a sequence of stable continuously related states change. At other times, however, the stable evolution behavior of the sliding system crosses a threshold whereupon a sudden change in contact conditions occurs as a result of instability.

This invokes a feedback loop that comprises the localized elevation of frictional heating, resultant localized bulging, increase in localized pressure owing to bulging, and further elevation of frictional heating owing to pressure increase. When this process leads to an accelerated change in the contact pressure distribution, the unexpected hot roughness of thermal distortion may grow unstably under some conditions, resulting in local hot spots and leaving thermal cracks on the disc.

To validate our thermomechanical model, we found in the literature, experimental test results, and measurement that have been made by Abu Bakar [19]. For this reason, a comparison in contact pressure distributions of inner pad was made between simulated and tested results.

We will first briefly discuss the experimental procedure, and then we will describe the method of measurements used by this author to explain the investigation of the methodology to show the clarity of the idea.

a) *Experimental setup and contact pressure test*

The contact pressure tests are conducted using an in-house disc brake dynamometer. The ventilated disc brake system of floating caliper design being investigated is shown in Fig. 24.

Brake pressure sensors enable precision measurements of many critical performance and safety measurements under both normal and extreme operating conditions. Tactile brake pressure sensors can be used to detect the pressure distribution across many braking. A customized tactile brake pressure sensors enhanced with a robust optical analysis system can collect valuable data for a number of challenging automotive applications, to provide a complete pressure map. Fujifilm Prescale brake pressure sensor® is disposable and easy to employ, able to withstand demanding pressures and high temperatures. Using the Presurex® Tactile indicating sensor film for clutch/brake applications is a cost-effective way to measure changes in pressure and distribution. Figure 25 present usage of pressure film placed on a brake pad.

In order to measure contact pressure distributions, a suitable type of sensor film should be chosen for a particular range of local contact pressure. In this work, Pressurex® Super Low (SL) pressure-indicating film, which can accommodate contact pressure in the range of 1 MPa is selected. The film needs to be cut to the shape of the brake pad for it to be well positioned in the pad/disc interface. Brake-line pressure at certain

Fig. 22 **a**–g Distribution of von Mises stress at different braking time: single piston with pad center-groove (*left*), single piston without groove (*center*), and double piston without pad groove (*right*) ▶

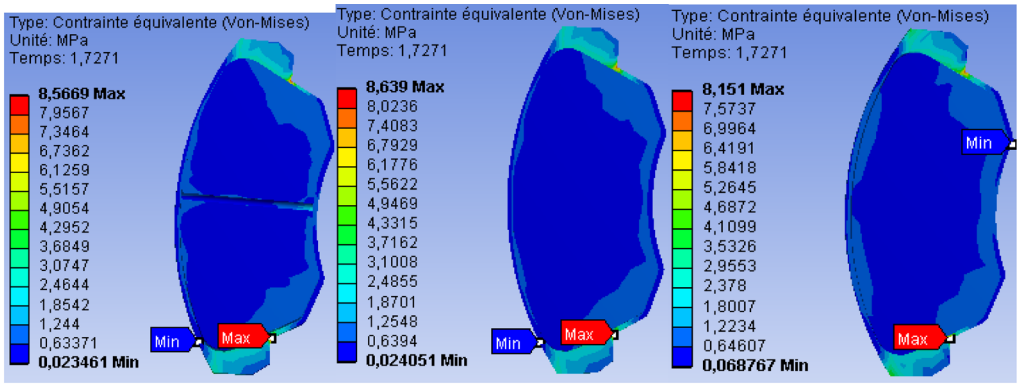

-a- *:* at time *t= 1.7s*

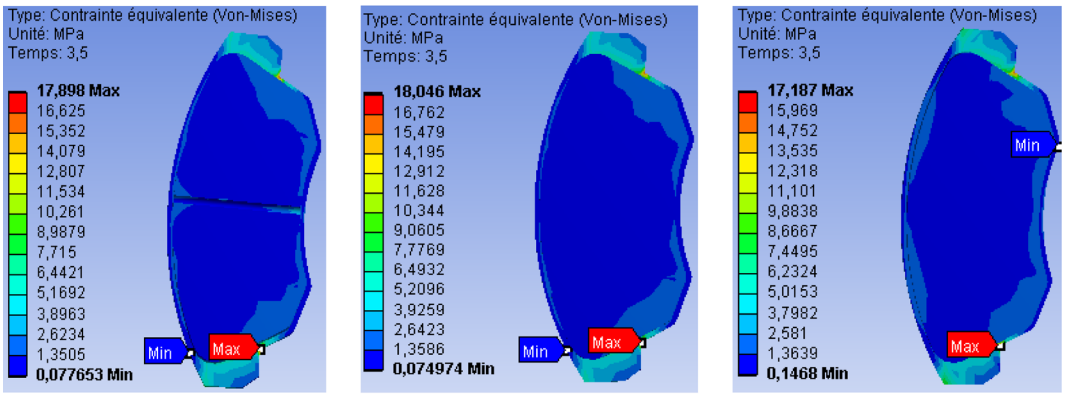

-b- *:* at time *t= 3.5s*

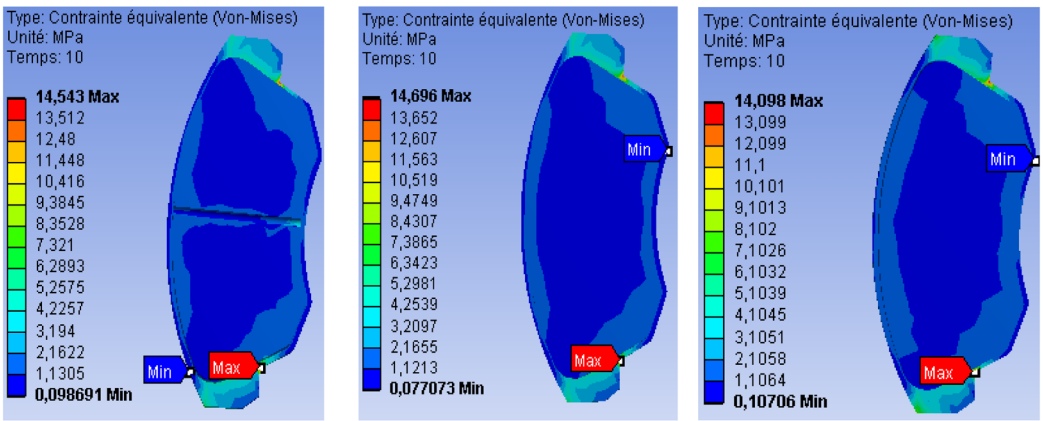

-c- *:* at time *t= 10s*

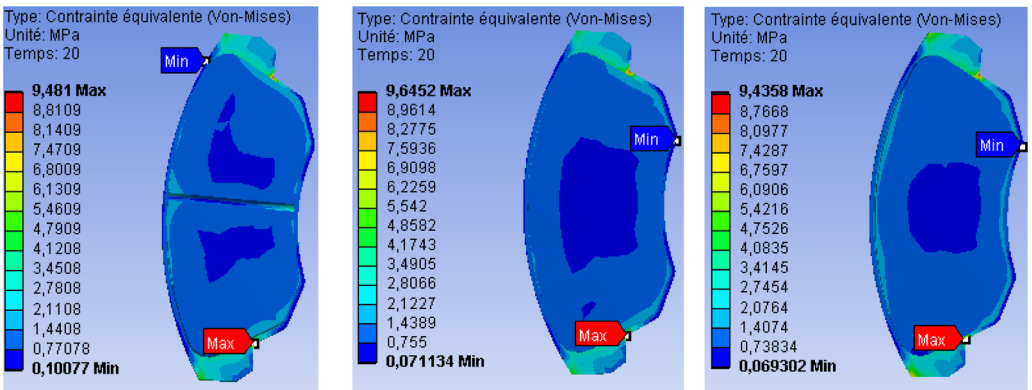

-d- *:* at time *t= 20s*

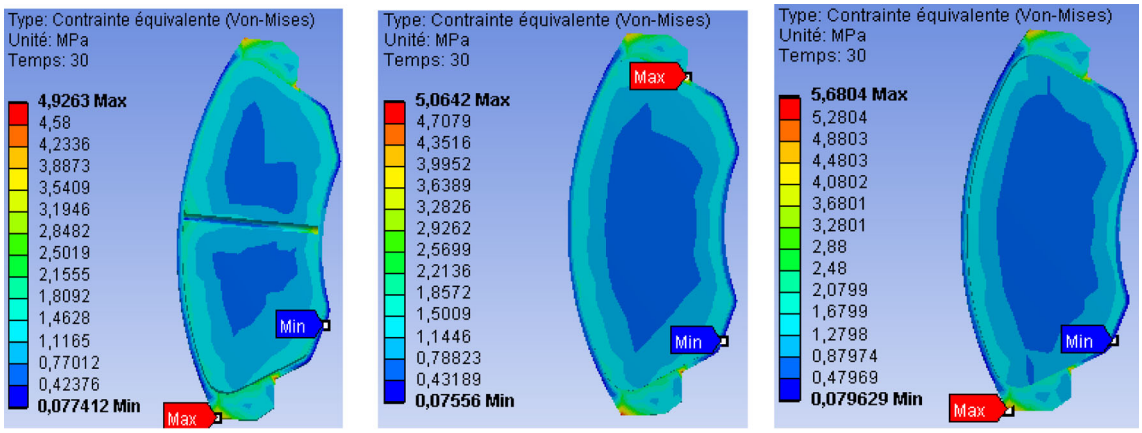

-e- *: at time t= 30s*

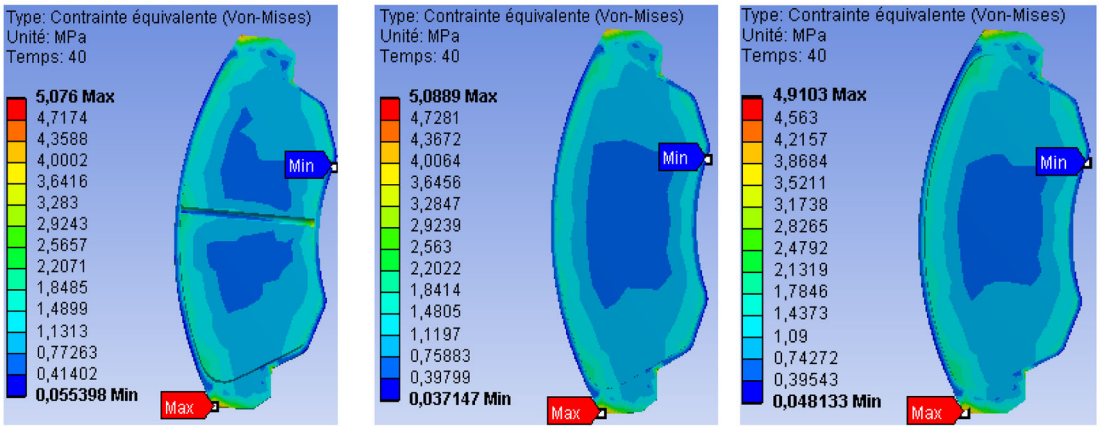

-f- *: at time t= 40s*

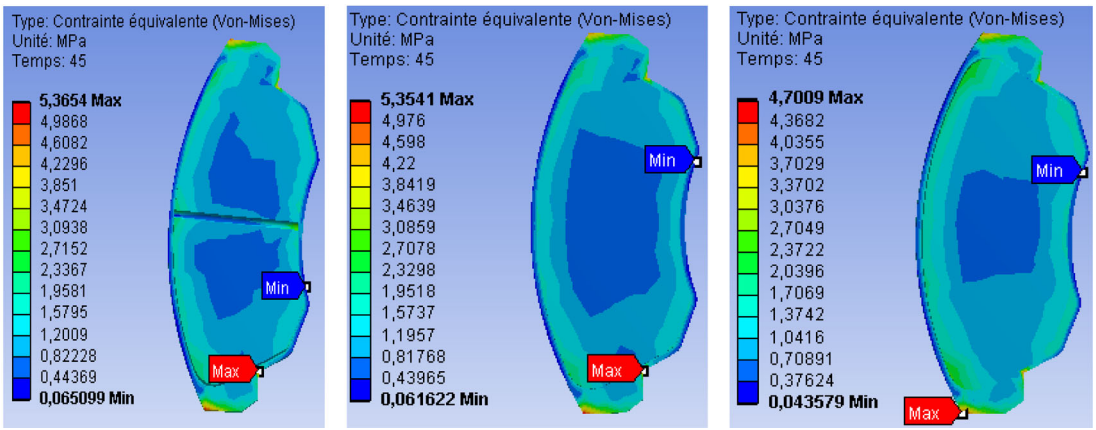

-g- *: at time t= 45s*

Fig. 22 continued.

levels is then applied to the disc brake for 45 s and then removed.

b) *Topaq® pressure analysis system*

It is not quite sufficient to describe contact pressure distributions by showing only the stress marks on the tested films. The contact pressure distributions should be measured qualitatively and quantitatively for comprehensive understanding. In doing so, a system called Topaq® Pressure Analysis system is used. Topaq® is a revolutionary stress measurement instrument for analyzing force distribution and magnitude. Topaq's user-friendly Windows-based software enables the characterization of how force is disbursed in any process or assembly where two surfaces contact or impact.

Table 5 Comparison of the results of the three pads design

Time (s)	von Mises stress (MPa)		
	Single piston with pad center-groove	Single piston without groove	Double piston without pad groove
1.7	8.5669	8.639	8.151
3.5	17.898	18.046	17.187
10	14.543	14.696	14.098
20	9.481	9.6452	9.4358
30	4.9263	5.0642	5.6804
40	5.076	5.0889	4.9103
45	5.3654	5.3541	4.7009

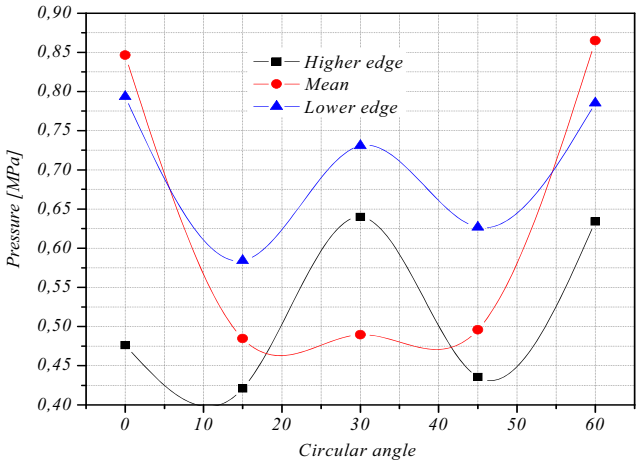

Fig. 23 Distribution of contact pressure along the lower, middle, and upper radius of the pad at time $t = 1.7$ s

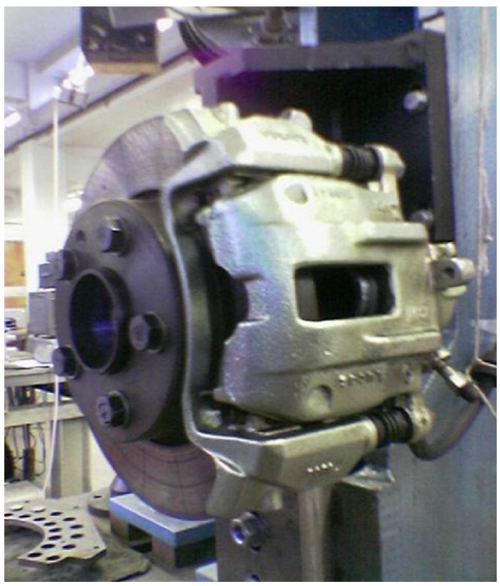

Fig. 24 A ventilated disc brake system

A Mitutoyo linear gauge LG-1030E and digital scale indicator are used to measure and provide reading of the brake pad surface topography as shown in Fig. 26.

Figure 27 plots the comparison results and shows the significant variation of the three curves. The contact pressure distribution of the pads increases remarkably when the thermal and mechanical aspects are coupled.

Also, it is clear from Fig. 27 that there is a good agreement between the numerical results and experimental data in thermomechanically coupled case. This gives an indication to brake engineers that in order to evaluate the brake performance, thermomechanical analysis should first be performed so that a realistic prediction can be achieved.

4 Conclusion

In this study, a disc-pad model has been analyzed using two approaches, namely, mechanical and thermomechanical analysis. In addition, three pad designs have been simulated to identify its influence on the stress distribution. From the prediction results, the following conclusions can be derived:

- Large deformation occurs at the outer radius of the disc.
- The presence of grooves in the pads unfavorably influences the mechanical behavior of a brake.

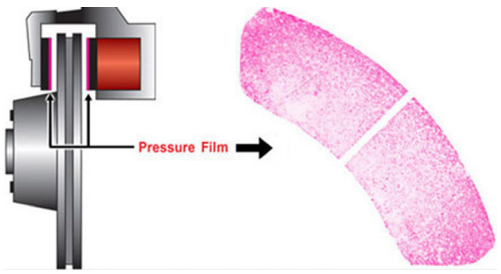

Fig. 25 Automotive use of break pressure sensor using Fujifilm Prescale® film before analysis

Fig. 26 An arrangement of brake pad surface measurements

- More uniform stress distribution is observed for a pad without groove and with double piston loading.
- Temperature significantly affects the structure and contact behavior of the disc brake assembly. Large deformation and high contact pressure are observed in the disc-pad model with the thermal effect.
- The numerical data obtained in this work, also supported by the experimental results.
- Based on the findings of this study, the following issues can be considered for further study:
- Thermomechanical stresses under repeated braking (settled stress-strain behavior)
- Fatigue analysis with dedicated material model
- Vibration analysis caused by stress components
- Wear and noise analysis of disc brake caused by thermally induced surface stress

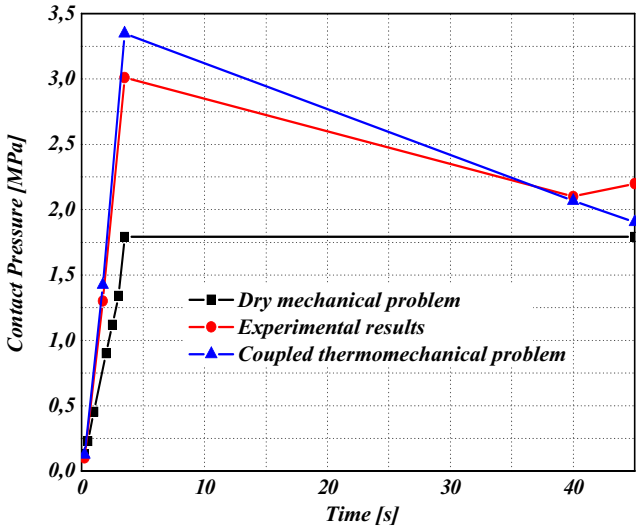

Fig. 27 Contact pressure of the inner pad

References

1. Belhocine A, Ghazaly NM (2015) Effects of material properties on generation of brake squeal noise using finite element method. Latin Am J Solids Struct 12 (8):1432–1447. doi:10.1590/1679-78251520
2. Lakkam S, Suwantaroj K, Puangcharoenchai P, Mongkonlerdmanee P, Koetniyom S (2013) Study of heat transfer on front- and back-vented brake discs. Songklanakarin J Sci Technol 35(6):671–681
3. Kumar ST, Vinodh S (2012) Novel design and analysis of a brake rotor. World Acad Sci Eng Technol 61:523–525
4. Agnihotri V, Chopra MK (2014) Optimized thermo-structural analysis of solid and vented disc brake using finite element method. J Mech Civil Eng (IOSR-JMCE) 11(4):40–49
5. Parab V, Naik K, Dhale AD (2014) Structural and thermal analysis of brake disc. Int J Eng Dev Res 2(2):1398–1403
6. Gao CH, Lin XZ (2002) Transient temperature field analysis of a brake in a non-axisymmetric three-dimensional model. J Mater Process Technol 129:513–517
7. Gao CH, Huang JM, Lin XZ, Tang XS (2007) Stress analysis of thermal fatigue fracture of brake discs based on thermomechanical coupling. Trans ASME J Tribol 129(3):536–543
8. Hwang, P., Wu, X., and Jeon, Y. B. (2008) Repeated brake temperature analysis of ventilated brake disc on the downhill road. In Proceedings of the 26th Annual Brake Colloquium and Exhibition, SAE paper 2008–01-2571
9. Choi JH, Lee I (2004) Finite element analysis of transient thermoelastic behaviors in disc brakes. Wear 257(1/2):47–58
10. Belhocine A, Bouchetara M (2012) Thermomechanical modelling of dry contact in automotive disc brake. Int J Therm Sci 60:161–170
11. Belhocine. A, Wan Omar W.Z (2016) Three-dimensional finite element modeling and analysis of the mechanical behavior of dry contact slipping between the disc and the brake pads. Int J Adv Manuf Technol, pp.1–17
12. Omolayo Petinrin M, Ogheneortega Oji J (2012) Numerical simulation of thermoelastic contact problem of disc brake with frictional heat generation. N Y Sci J 5(10):39–43
13. Basha Shaik AF, Srinivas CL (2012) Structural and thermal analysis of disc brake with and without crossdrilled rotar of race car. Int J Adv Eng Res Stud IJAERS 1(4) July-Sept:39
14. Khalid MK, Mansor MR, Abdul Kudus SI, Tahir MM, Hassan MZ (2011) Performance investigation of the UTeM eco- car disc brake system. Int J Eng Technol IJET-IJENS 11(06):1–6
15. Limpert R (1999) Brake design and safety, 2nd edn. Society of Automotive Engineering Inc., Warrendale, Pennsylvania, pp. 137–144
16. Mackin T, Noe SC, Ball KJ, Bedell BC, Bim-Merle DP, .Bingaman MC, Bomleny DM, .Chemlir GJ, Clayton DB, .Evans HA (2002) Thermal cracking in disc brakes. Eng Fail Anal 9:63–76
17. G.Oder, M. Reibenschuh, T. Lerher, M. Šraml, B. Šamec, I. Potrč (2009) Thermal and stress analysis of brake discs in railway vehicles. Adv Eng 3(1): ISSN 1846–5900
18. S.B. Sarip (2011) Lightweight friction brakes for a road vehicle with regenerative braking," Ph.D. Thesis, Engineering, Design and Technology, Bradford University
19. A R AbuBakar (2005) Modelling and simulation of disc brake contact analysis and squeal. PhD Thesis, Department of Engineering, University of Liverpool